Microswimmers in patterned environments

Giovanni Volpe,[*ab] **Ivo Buttinoni,**[b] **Dominik Vogt,**[b] **Hans-Jürgen Kümmerer**[b] **and Clemens Bechinger**[ab]

Tiny self propelled swimmers capable of autonomous navigation through complex environments provide appealing opportunities for localization, pick up and delivery of microscopic and nanoscopic objects. Inspired by motile cells and bacteria, man made microswimmers have been created and their motion in homogeneous environments has been studied. As a first step towards more realistic conditions under which such microswimmers will be employed, here we study, experimentally and with numerical simulations, their behavior in patterned surroundings that present complex spatial features where frequent encounters with obstacles become important. To study the microswimmers as a function of their swimming behavior, we develop a novel species of microswimmers whose active motion is due to the local demixing of a critical binary liquid mixture and can be easily tuned by illumination. We show that, when microswimmers are confined to a single pore whose diameter is comparable with their swimming length, the probability of finding them at the confinement walls significantly increases compared to Brownian particles. Furthermore, in the presence of an array of periodically arranged obstacles, microswimmers can steer even perpendicularly to an applied force. Since such behavior is very sensitive to the details of their specific swimming style, it can be employed to develop advanced sorting, classification and dialysis techniques.

1 Introduction

Brownian motion is the result of random collisions between a microscopic particle and the molecules of the surrounding fluid. In contrast, self propelled particles additionally take up energy from their environment and convert it into directed motion;[1 3] accordingly, their motion is a superposition of random fluctua tions and active swimming. Examples of such microswimmers range from chemotactic cells[4 6] to artificial systems powered, *e.g.*, by artificial flagella,[7 9] magnetic fields[10] or thermophoretic forces;[11] also, micron sized Janus particles have been realized where partial coating with a catalyst leads to non isotropic electrochemical reactions and thus to directed motion.[12 14]

Until now, most studies have concentrated on the behavior of microswimmers in homogeneous environments, where one typi cally observes a crossover from ballistic motion at short times to enhanced diffusion at long times, the latter due to random changes in the swimming direction.[15 17] However, self propelled particles often move in patterned environments, *e.g.*, inside the intestinal tract, which provides the natural habitat of *E. coli*,[5] or during bioremediation, where chemotactic bacteria spread through porous polluted soils.[18] In a similar fashion, artificial microswimmers must also reliably perform their tasks in complex surroundings, *e.g.*, inside lab on a chip devices[19] or living organisms.

Here, as a first step towards more realistic conditions under which such microswimmers are found and will be employed, we study their behavior in patterned surroundings where frequent encounters with obstacles become important. In particular, we investigate their motion within environments featuring simple topographical structures, such as a straight wall, a pore, and periodically arranged obstacles. In order to perform such experiments, we also develop a new species of artifical micro swimmers featuring a tunable active Brownian motion.

In Section 2, we present the novel species of microswimmers we have developed whose active motion is due to the local demixing of a critical binary liquid mixture and can be easily tuned by illumination. In Section 3, we present the behavior of such microswimmers in the presence of topological features, such as a planar wall (§3.1), a pore (§3.2), and periodical arrangements of obstacles (§3.3). Finally, we show how the dependence of the behavior of the microswimmers in the presence of periodically arranged obstacles can be used to sort them on the basis of their swimming properties (§3.4).

2 Self-diffusionphoresis in a critical mixture

Self propelled particles are obtained from paramagnetic silica spheres with radius $R = 2.13$ μm (Microparticles, SiO$_2$ MAG S1975) half coated with 20 nm thick gold caps (Fig. 1a). The gold surface is functionalized with COOH terminated thiols

[a]*Max Planck Institut fur Intelligente Systeme, Heisenbergstraße 3, 70569 Stuttgart, Germany. E mail: g.volpe@physik.uni stuttgart.de*
[b]*Physikalisches Institut, Universitat Stuttgart, Pfaffenwaldring 57, 70569 Stuttgart, Germany*
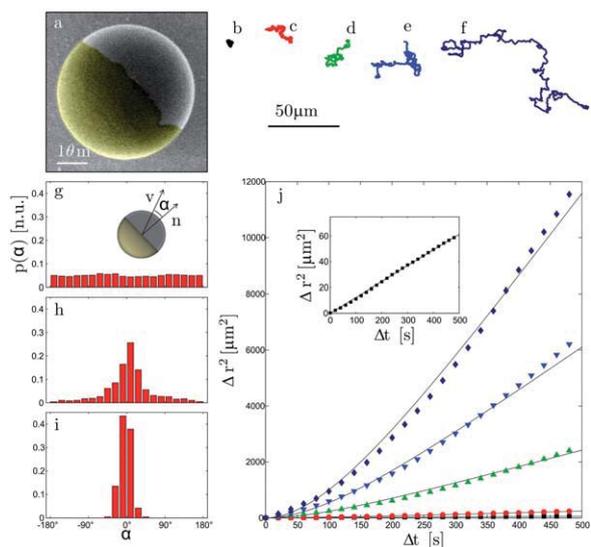
Fig. 1 The self-propulsion of Janus particles in critical mixtures. (a) A scanning electron microscopy image of a colloidal particle with a 20 nm thick gold cap (highlighted). (b–f) 2D trajectories (1000 s) of a Janus particle for illumination intensities $I =$ 0, 69, 92, 115, 161 nW μm^{-2} (respectively to b, c, d, e and f). (g–i) Probability distribution of the angle between the cap and the particle velocity for $I =$ 0 (g), 69 (h), and 138 nW μm^{-2} (i). (j) Experimentally determined mean square displacements (symbols) and relative fittings to eqn (1) (lines) for $I =$ 0, 69, 92, 115, 161 nW μm^{-2} (respectively squares, circles, up pointing triangles, down pointing triangles and diamonds). The inset is a magnification of the data for $I = 0$. The solid lines correspond to fits according to eqn (1), see also Table 1.

(11-mercapto-undecanoic acid) to render the caps strongly hydrophilic. When such Janus particles are suspended in a critical mixture of water and 2,6-lutidine[20] (0.286 mass of lutidine) below the critical temperature $T_c = 307$ K, they undergo normal Brownian motion (Fig. 1b). The base temperature of the sample cell is controlled by a thermostat and is adjusted below T_c. However, when the entire sample cell is homogeneously illuminated with light ($\lambda = 532$ nm) at low intensities I (<0.2 μW μm^{-2}), the particle's motion strongly depends on the incident light intensity, as shown in Fig. 1c–f. In particular, the trajectories become ballistic at short times, as is typically found for self-propelled objects.[15] To follow the particles' trajectories with video microscopy, their motion is vertically confined between two microscope cover slides kept 7 μm apart.

These particles are propelled by the local asymmetric demixing of a critical mixture upon illumination by light. Similarly to other mechanisms proposed in literature,[11–14] the propulsion can be tracked down to diffusiophoresis, which generally occurs when a particle is subjected to a concentration gradient within the solvent.[21] Here, such gradients are created by the particle itself (self-diffusiophoresis[22,23]) because the incident light is absorbed by the gold cap and thus leads to a local demixing of the binary solvent once the cap temperature exceeds T_c; the local demixing occurs only on the coated side of the particle, which is hotter. In the case of a hydrophilic cap this leads to an accumulation of the water-rich phase at the gold cap. The main advantage of this

mechanism is that very low light intensities can be used, since only a very small local increase of the temperature is needed in order to demix the critical mixture, permitting us to exclude optical forces and to accurately tune the active Brownian motion of the particle. Furthermore, since the demixing of the critical mixture is only local, the "fuel" driving the microswimmer regenerates once the particle has moved to a different region of the sample.

A homogenous illumination is obtained by scanning a highly defocused laser beam over the entire area of the sample (600 μm × 600 μm) using an acousto-optical deflector. The illumination power is tuned by adjusting the laser intensity. The typical illumination intensity $I < 0.2$ μW μm^{-2}, is low enough to permit us to exclude optical forces, which typically occur for $I > 10^4$ μW μm^{-2};[24] we furthermore have checked that in a non-critical solvent (water) or at temperatures $T \ll T_c$ the behavior of the Janus particles remains Brownian regardless of the illumination. We have also observed a similar behavior of the Janus particles by illuminating with a standard microscopy illumination on a bright-field microscope.

From the recorded videos, we also determined the particle's time-dependent propulsion direction **v** together with their current cap orientation **n** and the enclosed angle α (see inset of Fig. 1g). Fig. 1g–i show the normalized probability distribution $p(\alpha)$ for increasing illumination intensity I. Clearly, $p(\alpha)$ becomes strongly peaked around $\alpha = 0$ with growing I, which demonstrates that the propulsion force acts in the direction opposite to the gold cap. When the gold cap is made hydrophobic, the propulsion direction becomes reversed since then the lutidine-rich phase accumulates at the cap and thus leads to a change in the sign of the concentration gradient.

The analysis of the mean square displacements (MSD) clearly shows that the particles perform active Brownian motion.[15] The symbols in Fig. 1j show the experimentally determined MSD for the conditions of Fig. 1b–f. In the absence of illumination, the particles undergo normal Brownian motion, where the MSD equals $\Delta r^2 = 4D_0\Delta t$ (inset of Fig. 1j) with diffusion coefficient $D_0 = 0.031 \pm 0.006$ μm^2 s^{-1}. With increasing intensity, the MSDs clearly deviate from a diffusive behavior, and are well described by[15,17]

$$\Delta r^2 = \left[4D_0 + \frac{L^2}{\tau}\right]\Delta t + \frac{L^2}{2}\left[\exp\left(-\frac{2\Delta t}{\tau}\right) - 1\right], \qquad (1)$$

which generally characterizes the motion of self-propelled particles. Here, τ is the average timescale over which the trajectory direction is maintained. Accordingly, the average velocity of the particle is $v = L/\tau$[15] with L the swimming length, *i.e.* the average length of rather straight segments in the particle's trajectory. Due to the random changes in the particle's direction, for long times ($\Delta t \gg \tau$) eqn (1) leads to an effective diffusion with $D_{eff} = D_0 + L^2/4\tau$, while for short times ($\Delta t \ll \tau$) the particle's motion becomes ballistic with $\Delta r^2 \propto L^2\Delta t^2$. The values of the free fitting parameters τ and v for which best agreement with the data has been achieved are listed together with L and D_{eff} in Table 1. From this it becomes obvious that L increases (above some threshold value) linearly with the illumination intensity. In contrast, no significant variation of τ with I is observed. The value $\tau \approx 200$ s for which best agreement with the experimental

Table 1 Characterization of self propulsion. From the fit of eqn (1) to the measured MSD we obtain the intensity dependent average swimming speed v and time τ during which the swimming direction is maintained. From v and τ we calculate the swimming length $L \approx v\tau$ and the effective diffusion coefficient $D_{eff} \approx D_0 + L^2/4\tau$. The errors correspond to standard deviations

I (nW μm^{-2})	τ (s)	v (nm s^{-1})	L (μm)	D_{eff} (μm^2 s^{-1})
0				0.031 ± 0.006
46	220 ± 20	46 ± 5	10 ± 2	0.147 ± 0.029
69	190 ± 20	85 ± 7	16 ± 3	0.370 ± 0.069
92	190 ± 20	175 ± 20	33 ± 8	1.49 ± 0.42
115	220 ± 30	265 ± 33	58 ± 14	3.89 ± 1.01
138	240 ± 40	310 ± 28	74 ± 13	5.80 ± 1.49
161	230 ± 40	360 ± 27	83 ± 12	7.48 ± 1.86

data is obtained is close to the timescale of rotational diffusion $\tau_R = 1/D_R = 4R^2/3D_0$ with D_R the rotational diffusion coefficient. This yields $\tau_R = 188$ s for the $R = 2.13$ μm particles, which is indeed close to τ. Similar agreement (within $\pm 10\%$) between τ and τ_R has also been found for Janus particles with radii between $R = 1.0$ and 0.5 μm. This suggests that directional changes in the trajectories result from cap reorientations due to rotational diffusion.

3 Microswimmers in patterned environments

3.1 Encounters with a wall

When self propelled particles swim through a patterned medium, in particular for high swimming velocities, frequent encounters with obstacles will occur. Fig. 2a e show the interaction between a Janus particle and a wall. First the particle approaches the wall (Fig. 2a) and gets in contact (Fig. 2b). Then it slides along the wall (Fig. 2c) until rotational diffusion realigns the particle so that its orientation vector **n** points away from the wall and leads to particle detachment (Fig. 2d,e). Measuring the distribution of the particle wall contact time τ_c, we find a monotonic decrease as shown in Fig. 2f (bars). We also performed numerical Brownian dynamics simulations,[25] where the motion of the Janus particle is modelled by a superposition of random diffusion and ballistic motion with velocity v as inferred from Table 1. From the simulated particle trajectories we calculated the corresponding distribution $p(\tau_c)$ (line in Fig. 2f), which shows good agreement with the experimental data; in particular, in both cases the

average $\tau_c \ll \tau_R$ due to the angular distribution of the incoming particle direction. This suggests that the particle wall encounter mechanism is correctly described by this simple model and, in particular, that the rotational diffusion remains largely unaffected by the proximity to the wall.

3.2 Effects of confinement in a pore

The red/light grey trajectories presented in Fig. 3a e are typical of a microswimmer confined in a circular pore with diameter $r = 38$ μm. The various pictures correspond to various ballistic lengths and, therefore, light intensities (Table 1). In Fig. 3a, the particle moves diffusively exploring all the pore uniformly, as a consequence of its ballistic length being much shorter than the pore characteristic length, i.e. $L = 16$ μm $\ll r$. Similar results hold for shorter L and in particular for a non active Brownian particle for which L is due to the inertia of the particle and lays in the order of a few picometres.[26] The chances that the particle encounters the cavity wall in one of its straight runs increase as L gets longer. Once the particle touches the wall, it starts diffusing along the cavity perimeter until the rotational diffusion orients the cap towards the interior of the well, according with the process described in Fig. 2. As expected, the probability of finding the particle at the confinement wall strongly increases when L is significantly larger than r, e.g. $L = 74$ μm (Fig. 3d) and $L = 83$ μm (Fig. 3e). We have also confirmed these results with numerical simulations of self propelling particles (blue/dark grey trajectories in Fig. 3).

3.3 Deflection in a 2D periodic pattern

We have also investigated the behavior of self propelled particles in the presence of a two dimensional periodic pattern where straight unlimited swims are only possible along certain directions. We have chosen a structure made of a series of ellipsoidal pillars arranged in a triangular lattice (lattice constant $L_c = 35$ μm, Fig. 4a). Within such structures, long swimming cycles are only possible along two main directions: at $\pm 60°$ and $\pm 90°$ with respect to the y axis. Otherwise the motion is strongly hindered due to collisions with the obstacles. This leads to strong differences in the particle trajectories depending on their swimming length. In the presence of an additionally applied drift force, this permits us to separate the microswimmers according to their swimming behaviour. In our experiments a constant drift force acting on the paramagnetic particles in the y direction is
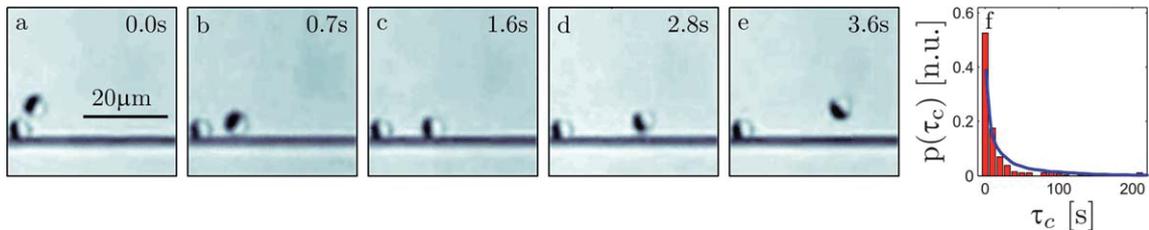

Fig. 2 An encounter between a microswimmer and a wall. (a e) Time series of snapshots demonstrating the approach (a), contact (b d) and detachment (e) of a Janus particle and a wall. The particle in the left corner is an irreversibly stuck particle that serves as a reference position. The contrast of (a e) has been enhanced for clarity. (f) Experimentally measured (bars) distribution $p(\tau_c)$ of the contact time between a microswimmer and a wall (I 115 nW μm^{-2}) for more than 250 encounter events. The line represents the result of a numerical simulation with L and τ taken from the experimental values of Table 1.

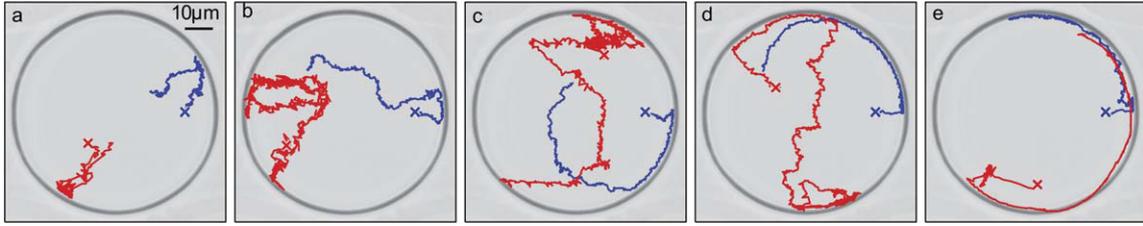**Fig. 3** Microswimmer in a confined geometry. The red/light grey lines represent measured trajectories of a 2.13 μm Janus particle moving in a circular well with diameter $r \approx 38$ μm for different illumination intensities corresponding to ballistic lengths (a) $L \approx 16$ μm, (b) $L \approx 33$ μm, (c) $L \approx 58$ μm, (d) $L \approx 74$ μm and (e) $L \approx 83$ μm. The blue/dark grey lines are numerically simulated trajectories. All trajectories were sampled over 600s.

generated by a magnetic field gradient; we remark that this force is independent of the orientation of the particles because these are sufficiently isotropic. From the average drift speed of a Brownian particle ($I = 0$ μW μm^{-2}), the drift velocity has been determined as $v_d = 0.97$ μm s^{-1}, which corresponds to a Stokes force of $F = 0.12$ pN.

The typical trajectory of a Brownian particle is shown in Fig. 4a. Because of the Péclet number $Pe \approx 1000$, the effect of the diffusion is rather weak and the particle meanders almost deterministically through the structure in the direction of F. For increasing swimming lengths, however, significant changes in the shape of the trajectories are observed. This becomes particularly pronounced for $L > L_c$, where the particles perform swimming cycles of increasing length along the diagonal channels (Fig. 4c, d). For $L = 83$ μm the propulsion becomes so strong that the particles partially move perpendicular to the drift force (Fig. 4e); occasionally even motion against the drift force can be observed.

The direction of the particle motion through the structure is characterized by the direction (with respect to the y axis) of the line connecting points of the trajectory separated by a distance of 100 μm. The probability distributions of these angles are shown by the red/light grey polar histograms in Fig. 4f–j. One clearly observes that with increasing L the propagation of particles along the direction of the applied drift becomes less likely, while

trajectories along ± 60°, *i.e.* along the directions that permit long swimming events, become more frequent. We remark that, differently from the deflection of Brownian particles in a periodic potential,[27–29] this mechanism relies on the dynamical properties of the microswimmers. We also compare these results with numerical simulations (blue/dark grey polar histograms in Fig. 4f–j), which show good agreement with the experimental data.

3.4 Sorting of microswimmers

With the additional possibility of varying the drift force, these observations can be exploited to spatially separate self-propelled particles with small differences in their individual swimming behavior. This is demonstrated in Fig. 5, where we show the deflection efficiency as a function of L, as defined by the probability that the mean particle trajectory is deflected by more than 30° after a travelling length of 100 μm. As symbols (lines) we have plotted experimental (simulation) data obtained for different drift forces. The black data (squares) correspond to $F = 0.12$ pN (Fig. 4). Here the deflection efficiency shows a strong increase around $L \approx 30$ μm and a flattening towards larger swimming lengths. The blue (diamonds) and red (triangles) data are obtained for $F = 0.06$ and 0.28 pN, respectively, and
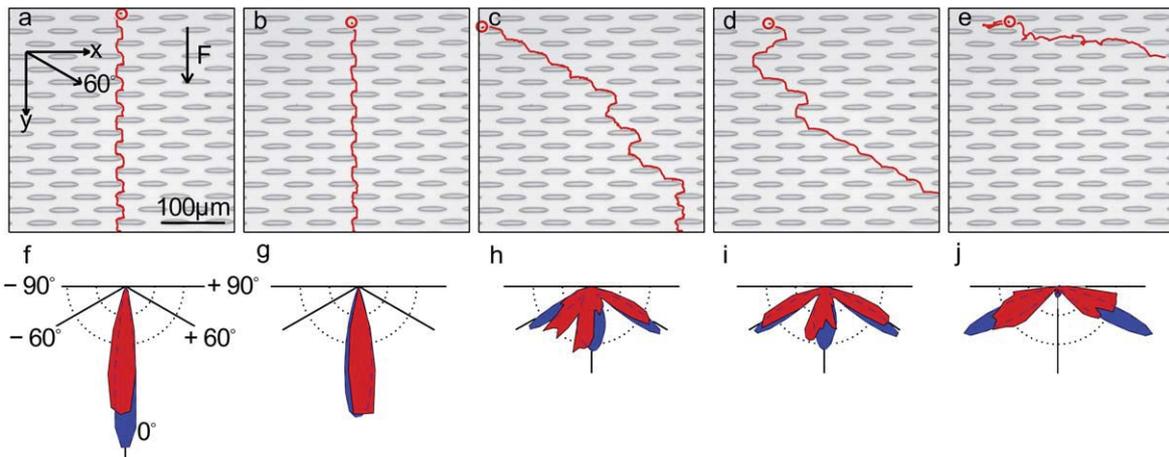

Fig. 4 Microswimmers in a patterned environment. (a–e) Typical trajectories of self-propelled particles moving through a triangular lattice (lattice constant $L_c \approx 35$ μm) of elliptical obstacles when a drift force $F \approx 0.12$ pN is applied along the y direction. (a) Brownian particle (no propulsion), (b) $L \approx 16$ μm, (c) $L \approx 24$ μm, (d) $L \approx 33$ μm and (e) $L \approx 83$ μm. (f–j) Corresponding histograms of the experimentally measured (red/light grey) and simulated (blue/dark grey) directions of the particle trajectories as defined by two points in the trajectory separated by 100 μm. The experimental histograms were obtained considering more than 100 trajectories in each case. The parameters for the simulations are taken from Table 1.
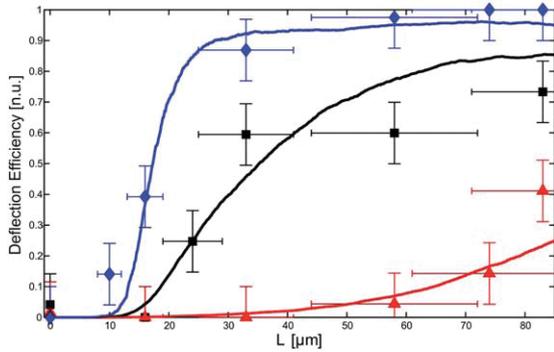
Fig. 5 Deflection efficiency of microswimmers. Measured probability that particles are deflected by more than $30°$ after a travelling length of $100~\mu m$ as a function of the swimming length L for various imposed magnetic drift forces F 0.06 ± 0.02 pN (diamonds), 0.12 ± 0.05 pN (squares) and 0.28 ± 0.12 pN (triangles). The solid lines are the results of numerical calculations. The experimental histograms were obtained considering more than 100 trajectories in each case. The parameters for the simulations are taken from Table 1.

demonstrate that the sorting efficiency strongly responds to variations in F. Accordingly, the deflection (transmission) of self propelled particles while crossing a patterned structure can be easily tuned by the appropriate choice of F.

We remark that the sorting mechanism discussed here can be directly applied to other self propelled objects. In these cases, drift forces can be created, *e.g.*, by electric fields or by a solvent flow through the device. Therefore, we expect that our method may find wider use as an efficient technique to characterize the behavior of motile cells and bacteria even when the details of their swimming behavior differs from those of the particles employed in this work (see, *e.g.*, Fig. 6). Compared to other concepts for the sorting of chemotactic bacteria, our strategy avoids the need for the creation of chemical gradients.[30,31]
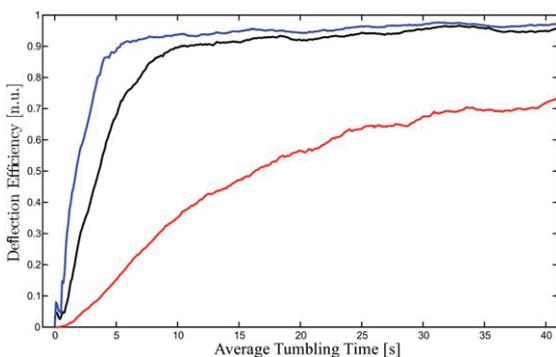

Fig. 6 Deflection efficiency of chemotactic bacteria. Differently from capped colloidal particles, chemotactic bacteria swim with constant speed and change their direction at a constant tumbling rate with the directional changes showing a peak around 30 degrees.[5] We simulated such bacteria with speed v $10~\mu m~s^{-1}$ as a function of their average tumbling time and simulated their deflection efficiency through the structure presented in Fig. 4 in the presence of a drift velocity along the y direction: $2~\mu m~s^{-1}$ (blue), $4~\mu m~s^{-1}$ (black) and $6~\mu m~s^{-1}$ (red). The deflection efficiency shows a qualitatively similar behaviour as Fig. 5 and thus confirms that the proposed sorting mechanism also applies to chemotactic bacteria.

4 Conclusions

In this article we have studied the behavior of microswimmers, *i.e.* active Brownian particles, with experiments and numerical simulations in the presence of patterned surroundings. We star ted exploring the interaction of a single microswimmer with a planar wall and then we moved towards more complex features, such as pores and periodical arrangements of obstacles. In the case of pores, we found that the active Brownian particles tend to spend more time by the confinement walls than their Brownian counterparts. In the case of periodical arrays of obstacles, we have found that active Brownian particles can steer even perpendicularly to an applied force; this behavior can be exploited to implement novel sorting, classification and dialysis techniques acting on the swimming style of the particles. In order to perform such experiments we needed to be able to alter the swimming behavior of the microswimmers without altering their other, *e.g.*, physical and chemical properties. We have, therefore, developed a new kind of microswimmer whose active motion is due to the local demixing of a critical binary liquid mixture and can be easily tuned by illumination. In comparison to other mechanisms proposed in the literature, the main advantage of our mechanism is that very low light intensities can be used, permitting us to exclude optical forces and to accurately tune the active Brownian motion of the particle. Furthermore, since the demixing of the critical mixture is only local, the "fuel" driving the microswimmer regenerates once the particle has moved to a different region of the sample.

Acknowledgements

References

1 R. F. Ismagilov, A. Schwartz, N. Bowden and G. Whitesides, *Angew. Chem.*, 2002, **114**, 674.
2 S. Ebbens and J. R. Howse, *Soft Matter*, 2010, **6**, 726.
3 F. Schweitzer, *Brownian Agents and Active Particles*, Springer, Berlin, 2003.
4 H. Berg and D. Brown, *Nature*, 1972, **239**, 500.
5 H. Berg, *E. coli in motion*, Springer, New York, 2004.
6 J. Mitchell and K. Kogure, *FEMS Microbiol. Ecol.*, 2006, **55**, 3.
7 R. Dreyfus, J. Baudry, M. Roper, M. Fermigier, H. Stone and J. Bibette, *Nature*, 2005, **437**, 862.
8 L. Zang, J. J. Abbott, L. Dong, K. Peyer, B. Kratochvil, H. Zhang, C. Bergeles and B. Nelson, *Nano Lett.*, 2009, **9**, 3663.
9 A. Snezhko, M. Belkin, I. Aranson and W. Kwok, *Phys. Rev. Lett.*, 2009, **102**, 118103.
10 P. Tierno, R. Golestanian, I. Pagonabarraga and F. Sagues, *J. Phys. Chem. B*, 2008, **112**, 16525.
11 H. R. Jiang, N. Yoshinaga and M. Sano, *Phys. Rev. Lett.*, 2010, **105**, 268302.
12 W. Paxton, A. Sen and T. Mallouk, *Chem. Eur. J.*, 2005, **11**, 6462.
13 N. Mano and A. Heller, *J. Am. Chem. Soc.*, 2005, **127**, 11574.
14 J. Gibbs and Y. Zhao, *Appl. Phys. Lett.*, 2009, **94**, 163104.
15 J. Howse, R. Jones, A. Ryan, T. Gough, R. Vafabakhsh and R. Golestanian, *Phys. Rev. Lett.*, 2007, **99**, 048102.
16 J. Palacci, C. Cottin Bizonne, C. Ybert and L. Bocquet, *Phys. Rev. Lett.*, 2010, **105**, 088304.
17 K. Franke and H. Gruler, *Eur. Biophys. J.*, 1990, **18**, 335.
18 R. Ford and R. Harvey, *Adv. Water Resour.*, 2007, **30**, 1608.

19 C. Chin, V. Linder and S. Sia, *Lab Chip*, 2007, **7**, 41.
20 C. Grattoni, R. D. C. Seah and J. Gray, *J. Chem. Eng. Data*, 1993, **58**, 516.
21 J. Ebel, J. Anderson and D. Prieve, *Langmuir*, 1998, **4**, 396.
22 R. Golestanian, T. Liverpool and A. Ajdari, *New J. Phys.*, 2007, **9**, 126.
23 R. Golestanian, T. Liverpool and A. Ajdari, *Phys. Rev. Lett.*, 2005, **94**, 220801.
24 A. Ashkin, *IEEE J. Sel. Top. Quantum Electron.*, 2000, **6**, 841 856.
25 P. Kloeden and E. Platen, *Numerical solutions of stochastic differential equations*, Springer, Berlin Heidelberg, 1992.

26 R. Huang, I. Chavez, K. M. Taute, B. Lukić, S. Jeney, M. G. Raizen and E. L. Florin, *Nat. Phys.*, 2011, **7**, 576.
27 M. MacDonald, G. Spalding and K. Dholakia, *Nature*, 2003, **426**, 421.
28 C. Reichhardt and C. O. Reichhardt, *Europhys. Lett.*, 2004, **68**, 303.
29 L. Huang, E. Cox, R. Austin and J. Sturm, *Science*, 2004, **304**, 987.
30 N. Jeon, H. Baskaran, S. Dertinger, G. Whitesides, L. V. D. Water and M. Toner, *Nat. Biotechnol.*, 2002, **20**, 826.
31 D. Englert, M. Manson and A. Jayaraman, *Nat. Protoc.*, 2010, **5**, 864.